3D Model of the *Escherichia coli* Multidrug Transporter MdfA Reveals an Essential Membrane-Embedded Positive Charge†

Nadejda Sigal,‡ Eyal Vardy,§ Shahar Molshanski-Mor,‡ Asa Eitan,‡ Yitzhak Pilpel,|| Shimon Schuldiner,§ and Eitan Bibi*,‡

Department of Biological Chemistry, Weizmann Institute of Science, Rehovot 76100, Israel, Alexander Silberman Institute of Life Sciences, The Hebrew University of Jerusalem, Jerusalem 91904, Israel, and Department of Molecular Genetics, Weizmann Institute of Science, Rehovot 76100, Israel

Received August 9, 2005; Revised Manuscript Received September 12, 2005

ABSTRACT: MdfA is an *Escherichia coli* multidrug transporter of the major facilitator superfamily (MFS) of secondary transporters. Although several aspects of multidrug recognition by MdfA have been characterized, better understanding the detailed mechanism of its function requires structural information. Previous studies have modeled the 3D structures of MFS proteins, based on the X-ray structure of LacY and GlpT. However, because of poor sequence homology, between LacY, GlpT, and MdfA additional constraints were required for a reliable homology modeling. Using an algorithm that predicts the angular orientation of each transmembrane helix (TM) (kPROT), we obtained a remarkably similar pattern for the 12 TMs of MdfA and those of GlpT and LacY, suggesting that they all have similar helix packing. Consequently, a 3D model was constructed for MdfA by structural alignment with LacY and GlpT, using the kPROT results as an additional constraint. Further refinement and a preliminary evaluation of the model were achieved by correlated mutation analysis and the available experimental data. Surprisingly, in addition to the previously characterized membrane-embedded glutamate at position 26, the model suggests that Asp34 and Arg112 are located within the membrane, on the same face of the cavity as Glu26. Importantly, Arg112 is evolutionarily conserved in secondary drug transporters, and here we show that a positive charge at this position is absolutely essential for multidrug transport by MdfA.

The simultaneous emergence of resistance in cells to many chemically unrelated drugs is termed multidrug resistance (Mdr).[1] Multidrug transporters that expel drugs from their intracellular targets represent a serious obstacle to successful anticancer and antimicrobial treatments (*1*, *2*). MdfA is an *Escherichia (E.) coli* Mdr transporter (*3*), which has served as a model in our studies of secondary Mdr transport. MdfA is a 410 amino acid residue long membrane protein of the Major Facilitator Superfamily (MFS) of secondary transporters (*4*), and it has close homologues in the pathogenic strains *Shigella flexneri* (99% homology) (*5*), *Salmonella enterica* serovar Typhi (90% homology) (*6*), and *Yersinia pestis* (73% homology) (*7*). Cells expressing MdfA from a multicopy plasmid exhibit multidrug resistance to a diverse group of lipophilic compounds, including monovalent cations, as well as zwitterionic and uncharged compounds (*3*, *8*, *9*). Transport experiments showed that MdfA is driven by the proton electrochemical gradient and functions as a (multidrug)(Na^+)-(K^+)/proton antiporter (*3*, *10*−*12*).

Several challenging questions regarding the multi-specific substrate recognition properties of MdfA and the bioenergetics and mechanism of its function as an Mdr transporter have been characterized to some extent using genetic and biochemical tools. However, better understanding of the mechanism requires 3D structural information. Limited structural information is available through the secondary structure model of MdfA, as constructed based on its hydrophobicity profile (*3*), gene fusion analysis (*13*, *14*), and several cysteine accessibility experiments (*15*). According to this model, MdfA is a typical MFS-related 12 transmembrane helix (TM) protein and it contains a single membrane-embedded, charged amino acid residue, Glu26, in the middle of the TMI (*13*, *14*). This glutamate constitutes an important part of the drug recognition pocket in MdfA (*9*, *13*). Additional determinants of multidrug recognition by MdfA, which were identified by genetic screens and mutagenesis, suggest the existence of a large and complex recognition pocket (*15*−*17*).

Recently, two high-resolution X-ray structures (*18*, *19*) and another 3D structure (*20*) were obtained for MFS-related solute-specific transporters. Despite their low sequence

† This work was supported by a grant from La Fondation Raphael et Regina Levy and by the Israel Cancer Research Foundation (ICRF) (to E.B.) and by Grant 2003-309 from the United States Israel Binational Science Foundation, Jerusalem, Israel (to S.S.). Y.P. is an incumbent of the Rothstein Career Development Chair in Genetic Diseases, and a Fellow of the Hurwitz Foundation for Complexity Sciences.

* Corresponding author. Fax: +972-8-9344118. Tel: +972-8-9343464. E-mail: e.bibi@weizmann.ac.il.

‡ Department of Biological Chemistry, Weizmann Institute of Science.

§ The Hebrew University of Jerusalem.

|| Department of Molecular Genetics, Weizmann Institute of Science.

[1] Abbreviations: CCCP, carbonyl cyanide *m*-chlorophenyl hydrazone; EtBr, ethidium bromide; LB, Luria−Bertani medium; Mdr, multidrug transporter; MFS, major facilitator superfamily; NTA, nitriloacetic acid; TM, transmembrane helix; TPP^+, tetraphenylphosphonium; HRP, horseradish peroxidase; ECL, enhanced chemiluminescence; DDM, β-dodecyl maltoside.

10.1021/bi051574p CCC: $30.25 © 2005 American Chemical Society
Published on Web 10/21/2005

similarity, the three proteins have very similar structures. These results, combined with several structural alignment studies of different MFS members (*21*−*25*), strongly support the hypothesis that all the MFS-transporters exhibit a similar fold (*26*). Following this suggestion, we analyzed the possible helix packing organization of MdfA using several prediction tools. The results show that MdfA may indeed have a fold similar to that of LacY and GlpT. Consequently, we performed structural alignment studies of MdfA, based on the known structures of LacY and GlpT. According to the predicted model, a potentially important positive charge (Arg112) is thought to be located within the membrane, at the periplasmic edge of the putative multidrug recognition pocket. This proposal was tested experimentally, and the results confirmed that a positive charge at position 112 is absolutely essential for MdfA function.

EXPERIMENTAL PROCEDURES

kPROT Analysis. Initially, we identified 200 homologues, separately for MdfA, LacY, GlpT, and also for a 12 TM transporter that does not belong to the MFS (NhaA) using PSI-BLAST as provided by the NSBI server using default parameters (BLASTP 2.2.6). These homologues were aligned by the ClustalX program (*27*) to produce a multiple alignment presentation. TMs of MdfA were defined using the PHD program (*28*) and refined based on the experimental results (*14*, *15*). Next, the kPROT algorithm (*29*) was implemented to predict angular orientation of the TMs, based on the multiple alignment. Variability vector was calculated based on BLOSUM62 matrix (*30*). Average kPROT values were calculated based on the value of each amino acid for each of the aligned TMs.

Generating and Refining an Alignment for the Homology Modeling. A PSI-BLAST search was done for each of the proteins used for the homology modeling. Sequences with identity ranging from 80% to 40% were selected for each of the proteins, and then they were aligned using T-COFFEE (*31*). The sequences of LacY, GlpT, and MdfA, aligned according to this procedure (gap only sites were omitted), were used to generate the initial models. An MdfA model constructed by averaging the two resolved structures of LacY and GlpT (a double model) will probably be closer to the truth than a model constructed individually by each of the two structures. However, for such a model to be generated, the spatial location of homologous residues from LacY and GlpT must be close. The alignment of GlpT and LacY from the multiple sequence alignment was compared to their structural alignment (sequence alignment of GlpT and LacY according to spatial location). The two procedures yielded very different alignments, implying that the current multiple alignment cannot be used for double modeling, because it would generate a poor model with many spatial paradoxes. According to the phylogenetic tree derived from the multiple sequence alignment, GlpT is the preferred template since it is closer to MdfA than LacY. Therefore, GlpT was used as the main template for constructing the MdfA model based on their multiple sequence alignment, with LacY added based on its structural alignment with GlpT (*32*). Finally, because of the low sequence homology, an additional fine-tuning was required based on the kPROT predicted angular orientation of the TMs of MdfA. Regions that generated large diversions from the Ramachandran plot were modeled according to one template (LacY or GlpT), which generates a better model.

Comparative Modeling. Comparative modeling was performed with Modeler 6.2 software (*33*). Modeling was performed with default "model" routine using LacY and GlpT (PDB ID 1PV6 and 4PW4, respectively) as templates, and the alignment of each of them with MdfA as an input. The first five residues and residues 227 to 239 in the L6-7 region of GlpT are not resolved in the structure (*19*) and were therefore replaced with gaps in the sequence and the alignments. The models were analyzed using PyMol. A Swiss pdb viewer was used to generate electrostatic potential surface. Procheck analysis was done using an RCSB PDB server.

Correlated Mutation Analysis. Initially, we identified homologues of MdfA by PSI-BLAST, as provided by the NSBI server with default parameters (BLASTP 2.2.10). Eighteen homologues with a similarity over 90% of the length of the protein were chosen, and ClustalX (*27*) was used to produce a multiple alignment presentation. This alignment was subjected to correlated mutation analysis (*34*), using the BLOSUM62 (*30*) similarity matrix. Only correlated mutations with a coefficient of 0.9−1.0 were selected.

Bacterial Strains and Plasmids. E. coli HB101 [*hsdS20* (r_B^- m_B^-), *recA13*, *ara-14*, *proA2*, *lacY1*, *galK2*, *rpsL20* (Smr^r), *xyl-5*, *mtl-1*, *supE44*, λ^-/F^-] was used for the propagation and preparation of various plasmid constructs. *E. coli* UT*mdfA::kan* or its leaky version UTL2*mdfA::kan* (Edgar and Bibi, unpublished data) were used in drug resistance and transport experiments. Cells transformed with plasmid pT7-5/*mdfA-6His* were used in resistance, expression, and transport assays. Cells transformed with plasmid pUC18/*pARA*/*mdfA-6His* were used for overexpression. *MdfA* was cloned with mutation in the 5′ 231-bp untranslated region of the chromosomal *mdfA* gene, which enhances the expression (*15*).

Site-Directed Mutagenesis. For genetic manipulations we used plasmid pT7-5/*mdfA-6His* and oligonucleotide-directed, site-specific mutagenesis by polymerase chain reaction (PCR). Each mutation was combined with an additional silent mutation that introduced a new restriction site. All the constructs were sequenced along the PCR product and the cloning joints, and by restriction analysis.

Drug Resistance Assays. Drug resistance was assayed on solid media, as described by Yerushalmi and Schuldiner (*35*). Briefly, *E. coli* UT*mdfA*::*kan* cells transformed with the mutants (pT7-5/*mdfA-6His* configuration) were grown at 37 °C in LB broth supplemented with the antibiotics ampicillin (200 μg/mL) and kanamycin (30 μg/mL) to 1.0 OD_{600} units. A series of 10-fold dilutions (10^{-1}−10^{-3}) were prepared, and a 4-μL aliquot of each dilution was spotted on plates containing different concentrations of the test drug. For pH-dependent resistance assays, the plates were also supplemented with 70 mM bis-tris-propane buffer at the desired pH. The ability of cells to form single colonies was recorded after 16−24 h incubation at 37 °C.

Western Blotting. Overnight cultures of *E. coli* UTL2*mdfA*::*kan* or UT*mdfA*::*kan* cells harboring pT7-5 (plain vector), or expressing 6His-tagged wild-type MdfA or the mutants were diluted (to 0.05 OD_{600} unit) in LB broth supplemented with ampicillin (200 μg/mL) and kanamycin (30 μg/mL), and grown to an OD_{600} of 1 unit. Bacteria were harvested,

and membranes were prepared as described previously (*36*). Membrane fractions (5−10 μg protein) were then subjected to SDS−PAGE (12.5%), and proteins were electroblotted to nitrocellulose membranes, which were incubated with India HisProbe-HRP, and probed by enhanced chemiluminescence.

Efflux of EtBr. EtBr efflux assays were conducted as described by Edgar and Bibi (*3*), with modifications. Overnight cultures of *E. coli* UT*mdfA*::*kan* cells harboring plasmid pT7-5 (vector alone) or the indicated pT7-5/mdfA-6His plasmids were diluted to 0.04 OD_{600} unit and grown at 37 °C in LB supplemented with ampicillin (200 μg/mL) and kanamycin (30 μg/mL) to 1.0−1.2 OD_{600} units. Aliquots of cells (0.3 OD_{600} unit) were pelleted, resuspended in 2 mL of KPi buffer (25 mM pH 7), and loaded with EtBr (5 μM) at 37 °C for 5 min in the presence of CCCP (100 μM). Loaded cells were then centrifuged, resuspended in the same buffer containing EtBr (5 μM) without CCCP, and then measured for fluorescence. After about 1 min in the fluorimeter, glucose was added (final concentration 0.4%). The EtBr efflux was monitored continuously by measuring the fluorescence, using excitation and emission wavelengths of 480 and 620 nm, respectively. CCCP was then added (as indicated) to abolish active transport.

Transport of Chloramphenicol. For chloramphenicol uptake assays, overnight cultures of *E. coli* UT*mdfA::kan* cells with different pT7-5/*mdfA-6His* constructs were diluted to 0.05 OD_{600} unit and grown at 37 °C in LB supplemented with ampicillin (200 μg/μL) and kanamycin (30 μg/μL) to 0.6 OD_{600} unit. The cultures were harvested and washed once with KPi buffer (50 mM pH 6.5). The cells were resuspended in the same buffer to 10 OD_{420} units and divided (50 μL aliquots). Following 2 min recovery at 37 °C in the presence of 0.2% glucose, transport was initiated by the addition of [^{3}H]chloramphenicol (0.2 μM). Transport was terminated by rapid filtration as previously described (*3*).

Preparation of Membranes. E. coli UTL2*mdfA*::*kan* cells harboring plasmid pUC18/pARA/*mdfA-6His* were grown at 37 °C in LB medium supplemented with ampicillin (100 μg/mL) and kanamycin (30 μg/mL). Overnight cultures were diluted to 0.07 OD_{600} unit, grown up to 1.0 OD_{600} unit, and induced with 0.2% arabinose for 1 h. A typical 12 L culture yielded 15 g (wet weight) of cells. Cell pellets were washed once in 0.8 L of 50 mM KPi (pH 7.5) supplemented with 5 mM $MgSO_4$, and pelleted by centrifugation (15 min, 5000*g*). Next, the cells were resuspended in 60 mL of the same buffer containing 1 mM β-mercaptoethanol, 30 μg/mL DNAse, and 0.5 mM pefablock, and passed three times through a French Pressure cell (15 000 psi) for disruption. Cell debris was removed by centrifugation (5 min, 8000*g*), and the membranes were collected by ultracentrifugation (2 h, 250000*g*). Finally, the pellets were resuspended and homogenized in 15 mL of buffer A (20 mM Tris-HCl, pH 8, 0.5 M NaCl, 5 mM imidazole, 10% glycerol). Aliquots of 1.8 mL containing ~100 mg of membrane proteins were snap-frozen in liquid nitrogen and stored at −80 °C.

Membrane Solubilization and Binding Assay. For solubilization, one aliquot of membranes was thawed at room temperature and DDM was added to 1.2%. The mixture was agitated gently for 30 min at 4 °C. Insoluble material was discarded by ultracentrifugation (1 h, 250000*g*), and the soluble fraction was mixed with Ni-NTA beads (10 μL/point) in a 15 mL tube. Next, the mixture was agitated gently for 30 min at 4 °C. The unbound material (sup) was discarded by pulse centrifugation in a tabletop centrifuge. The beads were then resuspended in 2.4 mL of buffer B (20 mM Tris-HCl, pH 7, 0.5 M NaCl, and 0.1% DDM), divided into 200 μL samples, and incubated (10 min, 4 °C) with 2.5 μM [^{3}H] TPP^+ (2 Ci/mmol). An aliquot of 180 μL of the resin−protein−[^{3}H] TPP^+ mixture was then transferred to a Promega Wizard minicolumn on top of a microfuge tube (1.5 mL) and centrifuged at 10000*g* for 20 s. Unbound (flow-through) material was discarded, and the MdfA-6-His-resin was resuspended in 100 μL of buffer B containing 350 mM imidazole. The radioactivity of this suspension was measured using liquid scintillation.

RESULTS

Angular Orientation of TMs. Previous studies (*26*) and structural alignment analyses (*21*−*25*), using as templates the X-ray structures of LacY (*18*) and GlpT (*19*), have suggested that the general fold of 12 TM MFS-transporters is conserved. However, the fact that sequence similarity is often very poor among proteins in this superfamily prohibits reliable structural alignment studies for many proteins, including the Mdr transporter MdfA. To overcome this problem, we have utilized the kPROT algorithm (*29*) as a powerful and potentially universal tool for membrane protein modeling. Initially, kPROT was used to predict the angular orientation of each TM of MdfA by determining which residues are exposed to the lipid phase and which ones are buried in the interior of a TM bundle(s). This is done by estimating the orientation propensities of amino acids, as derived from single-span versus multi-span membrane proteins. It is assumed that residues with a tendency to face the lipid milieu are more frequent in single-span proteins. The kPROT value for each residue is defined as a logarithm of the ratio of its proportions in TMs of single-span versus multi-span membrane proteins. We used a TM segment from a multiple alignment of 200 MdfA homologues for the input for each of the 12 TMs of MdfA (see Experimental Procedures). Figure 1 shows the predicted helical moments for all 12 TMs of MdfA. Most TMs of MdfA exhibit an angular orientation similar to that of the homologous ones, although several are highly scattered, usually reflecting poorly conserved sequences. However, there are several potentially interesting anecdotal exceptions that require further studies. The angular orientation of TMIIX and its homologues is conserved, despite sequence divergence. In contrast, although TMIII is relatively highly conserved in sequence, it shows a scattered angular orientation. A possible explanation for these differences would be that, unlike TMIII, TMIIX might play an important structural role in these transporters. Importantly, as suggested from the findings in Figure 1, residues of importance for multidrug recognition by MdfA are usually found in protein−protein interacting surfaces. Interestingly, for 9 of the TMs, where a relatively narrow set of orientations is predicted for most of their TM homologues, the variability helical moments (indicating the direction of most variable residues) are clearly oriented toward their predicted membrane-exposed aspects.

We further conjectured that the extent to which an entire TM is either buried or lipid-exposed might be predicted by the average kPROT values of the involved residues. Figure

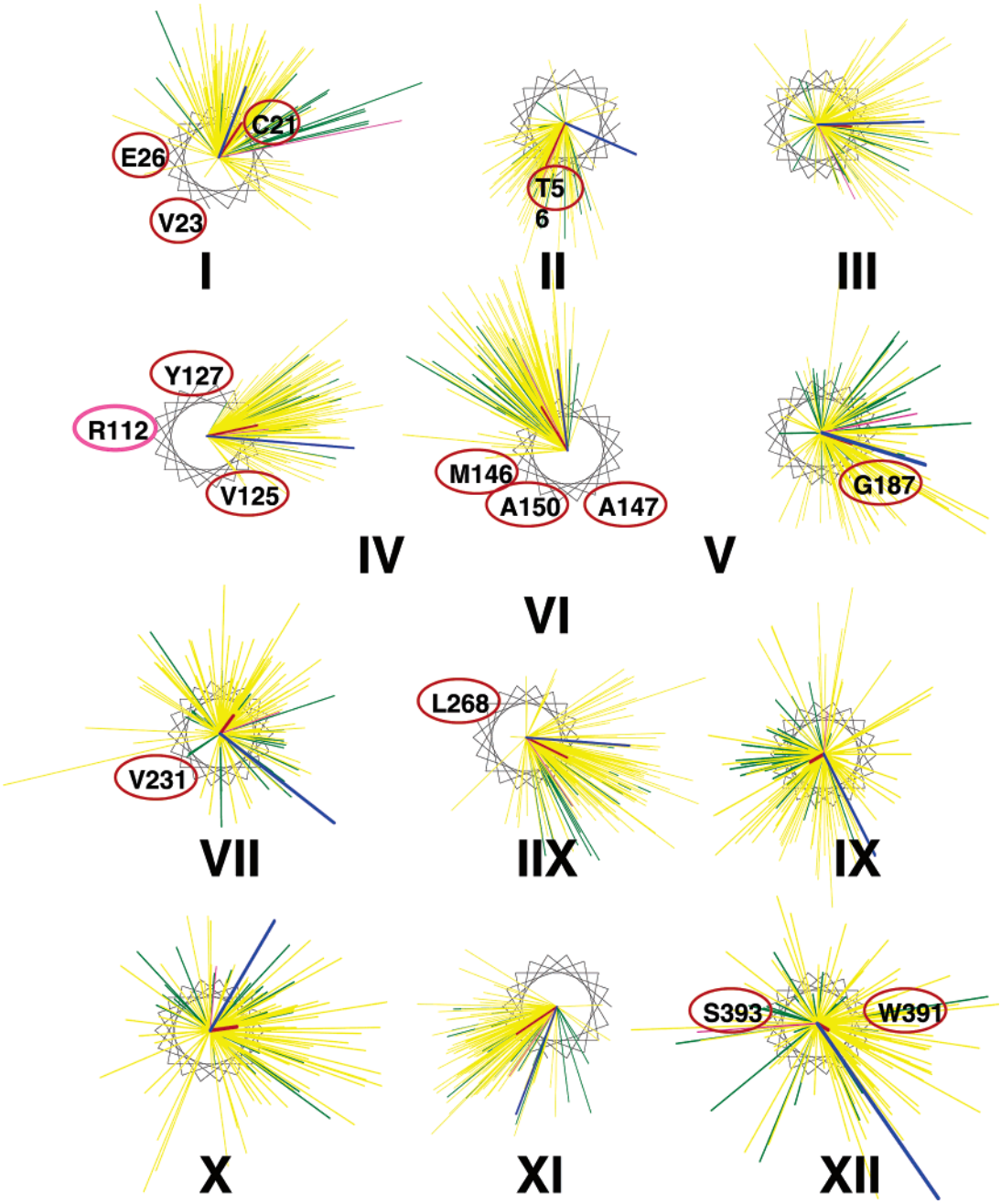

FIGURE 1: Prediction of the angular orientations of TMs in MdfA. TMs are represented as helical wheel viewed from the cytoplasm. Helical moments were calculated by kPROT (*29*) for MdfA (magenta), for 50 of its closest homologues (green), for the other 149 homologues (yellow), for the mean of all 200 homologues (red), and for a variability vector (blue). Residues of known functional importance are circled in red, except for Arg112, which is circled in magenta. In most cases, the important residues are predicted to be in protein−protein interaction faces.

2 shows the average kPROT value for each TM family, and according to these results, TMs III, VI, IX, and XII are the most membrane-exposed TMs in MdfA. Interestingly, a similar pattern of membrane-exposed TMs is found in the 3D structures of GlpT and LacY, suggesting that MdfA may indeed have a similar membrane organization. To test the precision by which kPROT predicts angular orientations and evaluate the notion that MdfA has a similar pattern of membrane-exposed TMs as GlpT and LacY, we also performed kPROT calculations for LacY and GlpT (Supporting Information). Importantly, kPROT performs very accurately for GlpT, since the mean moment deviates only slightly from that observed experimentally (mean deviation 22° ± 16°). For LacY, high scattering was observed with several TMs, although the mean moment fits the experimental data quite well (mean deviation 56° ± 41°, with the large deviations observed for external helices). Figure 2 shows also the average kPROT values of the TMs in GlpT and LacY. Remarkably, as with MdfA, TMs III, VI, IX, and XII, of LacY and GlpT, are also the most membrane-exposed TMs. Although the exact pattern of average kPROT values for TMs in the three transporters is not identical, a significant correlation exists (a correlation coefficient of 0.66 for LacY-GlpT; 0.77 for MdfA-GlpT; and 0.67 for MdfA-LacY). These results are in accordance with phylogenetic terms since GlpT is closer to MdfA than LacY (data not shown). Collectively, these results strongly support the suggestion that MdfA, LacY, and GlpT have similar helix packing.

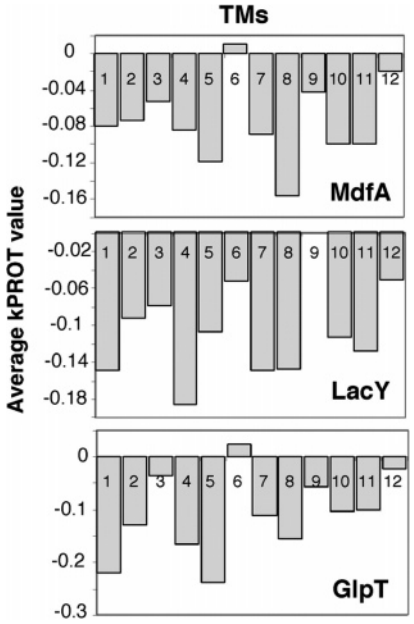

FIGURE 2: The average kPROT value of TMs in MdfA, LacY, and GlpT. The average kPROT value was calculated considering all the amino acids in all of the 200 homologues of each protein for the indicated TM. Gaps were excluded from the calculation. More negative value indicates TMs that are more buried in the protein interior. Correlation coefficients are 0.66 for LacY-GlpT; 0.77 for MdfA-GlpT; 0.67 for MdfA-LacY.

Finally, similar analysis with the MFS-unrelated 12 TM protein NhaA revealed an insignificant correlation of its average kPROT values with those of LacY, GlpT or MdfA (correlation coefficients of 0.02−0.3) (data not shown). Indeed, the 3D structure of NhaA shows that it has a membrane fold that differs from that of the MFS transporters (*37*).

Structural Alignment of MdfA. We performed 3D homology modeling studies of MdfA using the resolved X-ray structures of GlpT and LacY as templates (Figure 3A,B). Because of the low similarities at the level of amino acid sequence, the preliminary multiple sequence alignments of these proteins were manually improved using the kPROT-predicted membrane-facing vectors for all TMs. Ramachandran plot analysis performed by PROCHECK revealed that 96.9% of the non-glycine and non-proline residues are in the core and allowed regions, 1.7% in generously allowed regions, and only 1.4% in disallowed regions located mostly in loop regions, which are not expected to be perfectly predicted for membrane proteins by structural alignment. All main-chain parameters are within the bandwidth of a typical value. The overall *G*-factor is −0.1.

According to the 3D model of MdfA, it consists of N- and C-terminal domains, sharing a pseudo-2-fold symmetry. In agreement with the kPROT prediction, TMs I, II, IV, V, VII, IIX, X, and XI form a central cavity in the transporter; they are surrounded by helices III, VI, IX, and XII, which are facing the membrane. The membrane topology of MdfA and the charge distribution (see Figure 3C,D) in the periplasmic (negative) and cytoplasmic (positive) loops is generally consistent with previously constructed secondary structure models (*3*, *14*). However, an important difference is clearly apparent: in general, the TMs in the 3D model are longer than those predicted previously. The most significant differences are found in TMI and TMIV, where charged residues previously predicted to be periplasmic are located within the membrane. Specifically, according to the 3D model of MdfA, Glu26 (TMI), Asp34 (TMI), and Arg112 (TMIV) are all found within the membrane-embedded domain of the protein (Figure 4A). Consequently, unlike in previous predictions, Glu26 is located in the cytoplasmic half of TMI. As will be shown later, these findings may have important functional implications.

According to the 3D model of MdfA, its internal cavity is surrounded by TMs of the 2 halves of the protein. Interestingly, this cavity is negatively decorated by the acidic residues Glu26 and Asp34 in TMI, with a possible contribution of the cytoplasmic acidic residue Glu132, located in the loop between TMIV and V. This negatively charged cavity forms a distinct "hole" in the generally basic cytoplasmic face of the protein (Figure 3C,D). Previous genetic and biochemical studies have already revealed the importance of Glu26 as a substrate recognition determinant (*9*, *13*, *15*). Moreover, a role for Asp34 and Glu132 in substrate recognition has also been recently identified (*17*). We therefore suggest that the observed cavity represents the putative multidrug recognition pocket of MdfA.

Correlated Mutation Analysis. Correlated mutation analysis usually identifies structurally interacting residues (*34*). The key assumption here is that when two residues interact with each other, mutations in one residue will be complemented by compensatory mutations in the other residue, and as a result, this pair of residues will exhibit correlated mutational behavior. First, the exchange matrix for each position is defined by quantifying the similarity of residues observed at this position in the multiple alignment. Next, the correlation coefficient of the exchange matrices at any two positions is calculated. Correlated positions with a coefficient above a certain threshold (see methods) are selected. As input to the algorithm, we used a multiple alignment of 18 proteins, which show homology to MdfA over 90% of their sequences. The results of this analysis revealed important general information about the functional domains of MdfA (Figure 5). First, the distribution of intradomain pairs is surprising. Although as much as 78 correlations were identified between residues in the N-terminal half of MdfA, only 23 were found in the C-terminal half of MdfA. These results suggest that the structure of the C-terminal half and the inter TM interactions in this region are much less stringent than those in the N-terminal half of MdfA. Functionally, as also confirmed by genetic and biochemical studies, multidrug recognition is predominantly mediated by the N-terminal half of MdfA (*15*). Moreover, according to the correlated mutation analysis, the loop connecting TMX with TMXI has strong interactions with TMs that form the multidrug recognition pocket, which is also in agreement with genetic and biochemical studies (*16*) (see below). Importantly, these conclusions could not be predicted based solely on the 3D model of MdfA.

Comparison of the Experimental Results with the 3D Model of MdfA. Interestingly, genetic studies have shown that a negative charge at position 335 of MdfA (Val335Glu) functionally complements charge neutralization at position 26 (Glu26Thr) (*16*). Cross-linking experiments suggested a distance of approximately 10 Å between these two residues (Glu26 and Val335). These results are remarkably consistent with the predicted 3D model of MdfA. In this model, Glu26

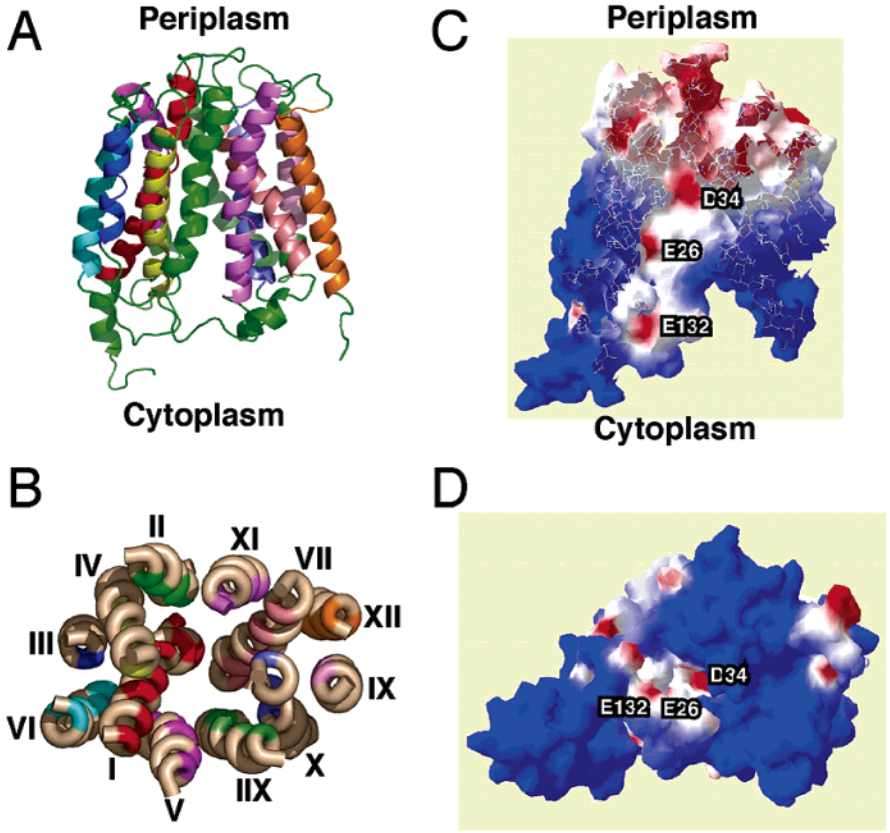

FIGURE 3: 3D model of MdfA. (A) The overall structure in ribbon representation viewed parallel to the membrane. (B) Ribbon representation of MdfA viewed along the plane of the membrane from the cytoplasmic side. In both (A) and (B) the color code used for TMs: I, red; II, green; III, blue; IV, yellow; V, magenta; VI, cyan; VII, salmon; IIX, lime; IX, pink; X, slate; XI, violet; XII, orange. For clarity the loop regions are omitted. Cα of the residues predicted by kPROT to point to the protein interior in each TM is also colored as indicated. (C, D) The surface model and the hydrostatic potential were calculated with the Swiss pdb-viewer. The polar surfaces are colored blue (positively charged) and red (negatively charged). (C) The negative groove formed by TMI, viewed parallel to the membrane. Slab of 20 Å is used for clarity. (D) The negative decoration of the cavity as viewed along the membrane normal from the cytoplasmic side.

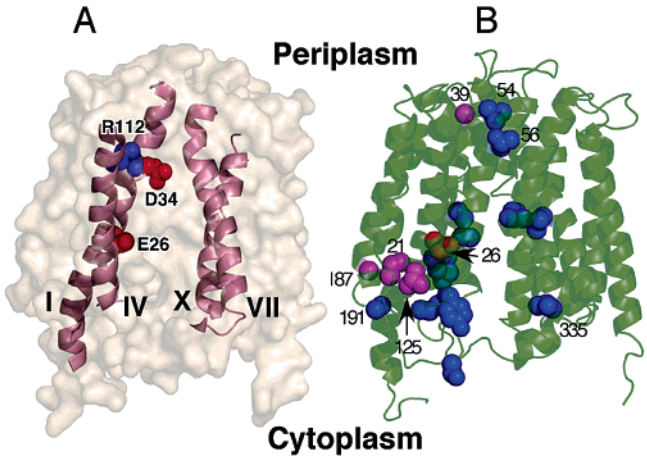

FIGURE 4: The 3D model of MdfA as viewed parallel to the membrane. (A) Glu26 and the two newly identified membrane-embedded charged residues are indicated and shown in the space-filled representation. Helices I, IV, VII, and X are presented for clarity. The surface model is calculated with the PyMol program. (B) Second-site mutations that restored the function of inactive Glu26 mutants (*15*, *16*) are shown in space-filled representation. Residues inaccessible from the putative substrate binding pocket are shown in magenta.

and Val335 are located at opposite sides of the cavity, pointing toward the interior (the proposed multidrug recognition pocket), and the calculated distance between them is approximately 13 Å (see Figure 4B).

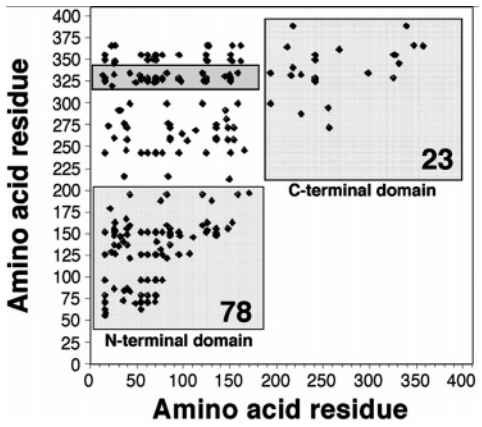

FIGURE 5: Correlated mutation map of MdfA. 18 homologues with a similarity over 90% of the protein length were used to produce a multiple alignment presentation. This alignment was subjected to correlated mutation prediction as developed by A. Valencia (*34*). Correlated mutations with coefficient of 0.9−1.0 were selected. The loop X−XI is highlighted in gray, and N- and C-terminal domains are highlighted in light gray. The number of intradomain correlated mutations in the C-terminal and N-terminal domains of MdfA is indicated.

Additional genetic screens with MdfA revealed several second site mutations that restored the function of inactive Glu26 mutants (*15*). These sites are thought to be involved directly or indirectly in multidrug recognition. To test this proposal, we marked the positions of these amino acid residues on the 3D model of MdfA. As shown in Figure

4B, most of these mutations point into the interior of the putative multidrug recognition pocket of MdfA. Three residues, Gly39, Val54, and Thr56, form a cluster in the periplasmic part of TMI and II, at the closed end of the cavity, whereas others (residues Cys21, Val23, Val125, Tyr127, Ala128, Ser133, Met146, Ala147, Ala150, Val231, and Leu268) are scattered throughout the cavity, mostly in its cytoplasmic portion. However, there are also several exceptions, specifically regarding residues Gly187 and Ala191 in TMVI, which are found behind TMI. These residues may have indirect conformational effects on substrate recognition via interactions with TMI.

Cysteine accessibility to hydrophilic reagents usually serves as a tool for identifying residues that are not buried in the membrane. Single cysteine mutants in MdfA, which were constructed based on the results of the second-site mutation screens, were tested in the accessibility assay (*15*). According to the 3D model of MdfA, moderately and highly accessible mutants are indeed found within the hydrophilic loops (residues Ser204 and Ser133), at the edges of TMs (residues Val54, Tyr127, Ala128, Ala191, Val335) or pointing toward the interior of the cavity (residue 147). Also in accordance with the model, the inaccessible mutants Val23, Glu26, Val 231, and Leu268 are located in the middle of the TMs. Finally, despite their location at the edges of TMs, several residues are not reactive (Gly39, Cys21, Val125, and Gly187). As shown in Figure 4B, these residues are putatively buried within the protein and thus might not be accessible for the chemical modification.

Studying the Role of Arg112. As noted, the 3D model of MdfA revealed yet another previously unpredicted membrane-embedded charge, Arg112 inside TMIV. This arginine is the most evolutionarily conserved residue in MdfA, and a similar membrane-embedded site (near the periplasm) was predicted for analogous arginines in the MFS transporters TetA and rVMAT2 (*21*). Consequently, as a working hypothesis, we postulated that Arg112 might have an important functional role in MdfA. Preliminary studies with Arg112 replaced by a cysteine supported this suggestion (data not shown). Therefore, further studies have been carried on in order to examine the possibility that Arg112 is indeed functionally important. To this end, in addition to the original Arg112Cys mutation, other substitutions were constructed. At the same time, the following issues were addressed: (i) the importance of the positive charge, and (ii) the importance of the size of the amino acid residue at position 112. Accordingly, the following mutations were constructed by PCR mutagenesis: Arg112Met, Arg112Gln, and Arg112Glu (mainly testing the charge issue); Arg112Lys and Arg112His (testing the size); Arg112Met or Arg112Gln also introduced hydrophobic or hydrophilic residues, respectively. The mutants were expressed at levels comparable to that of the wild-type MdfA, except for Arg112Glu, which was poorly expressed (Figure 6A). The effects of the various Arg112 mutations on the biological function of MdfA were tested by growth inhibition experiments. Figure 6B shows that mutants Arg112Cys, Arg112Met, Arg112Gln, and Arg112Glu did not grow on any of the test drugs. In contrast, the conservative mutant Arg112Lys did confer some resistance to thiamphenicol and benzalkonium, and to a lesser extent also against chloramphenicol, EtBr, ciprofloxacin, and TPP^+. Surprisingly, however, the most active mutant was Arg112His, which

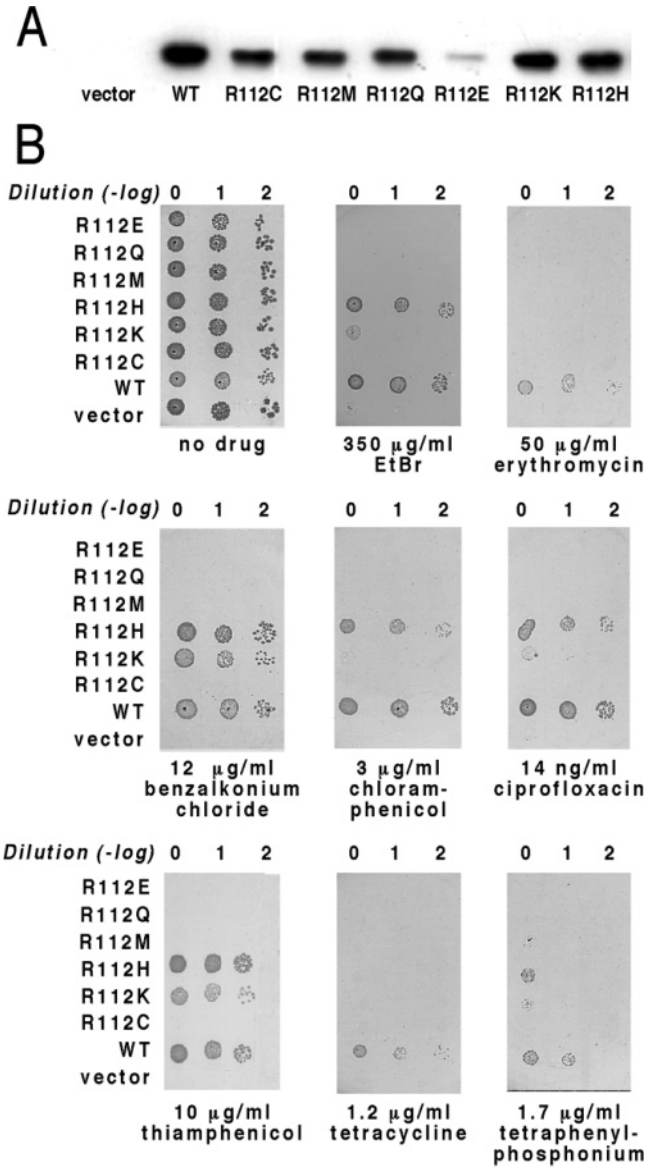

FIGURE 6: Characterization of R112 mutants. (A) Expression of the Arg112X mutants of MdfA. Membranes were prepared from cells expressing the indicated 6-His tagged mutants and analyzed by Western blotting. (B) Multidrug resistance phenotype of MdfA and mutants. *E. coli* was transformed with plain vector (vector), or plasmids encoding wild-type MdfA (WT), or Arg112 mutants. Cells were diluted (as indicated) and spotted on LB agar plates with or without the indicated drug. Plates were visualized after ~20 h at 37 °C.

exhibited high activity against many of the test compounds (except for erythromycin and tetracycline). The observation that only the MdfA mutants Arg112Lys and Arg112His were functional thus suggested that a positive charge at position 112 is required for transport activity.

Drug resistance assays provided indirect information about the activity of the R112 mutants of MdfA. To evaluate these observations further, we tested the activity of the mutants directly by drug transport assays. As shown in Figure 7A, cells expressing mutants Arg112Cys, Arg112Met, Arg112Gln, and Arg112Glu were unable to expel EtBr better than control cells with plain vector. However, cells expressing Arg112Lys showed a low but significant EtBr efflux activity, and cells expressing Arg112His showed efficient EtBr efflux that was only slightly lower than that mediated by wild-type MdfA.

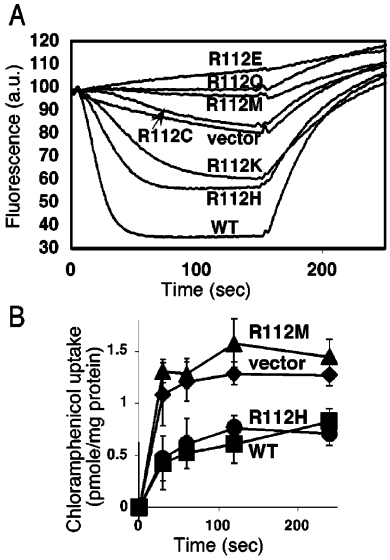

FIGURE 7: Transport activity of the Arg112 mutants of MdfA. (A) Cells expressing the indicated mutants were loaded with EtBr, energized with glucose (0.4%), and the EtBr efflux was monitored continuously in the fluorimeter. (B) [^{3}H]Chloramphenicol transport was assayed by rapid filtration with *E. coli* expressing wild-type MdfA (WT) (■), Arg112Met (▲), or Arg112His (●) mutants, or plain vector (vec) (◆). The experiments were performed in triplicate.

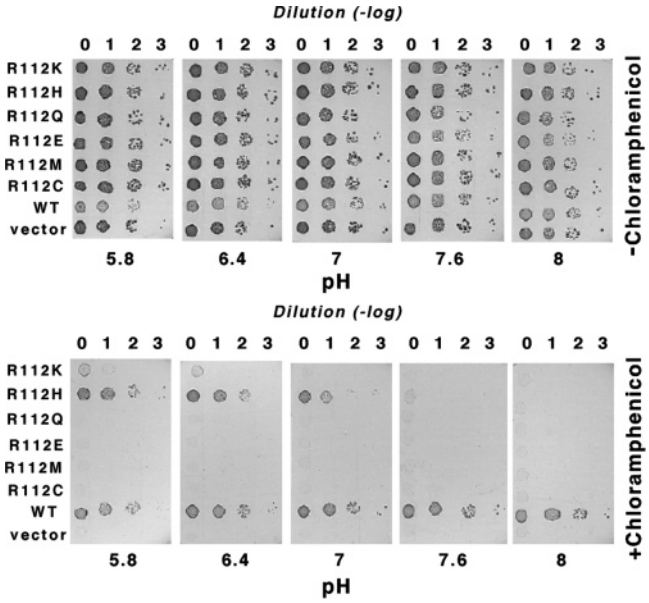

FIGURE 8: Chloramphenicol resistance assays under different pH conditions. *E. coli* was transformed with plain vector (vector), or plasmids encoding wild-type MdfA (WT), or Arg112 mutants. Cells were diluted (as indicated) and spotted on LB agar plates containing bis-tris propane at the indicated pH. Upper panel: plates without any drug. Lower panel: plates with chloramphenicol (3.5 μg/mL). Plates were visualized after ~20 h at 37 °C.

Similar results were obtained in chloramphenicol transport (Figure 7B): Arg112Met mutant is totally inactive, while Arg112His mutant has wild-type activity. Taken together, the transport and drug resistance results support the notion that a positive charge at position 112 is required for MdfA function.

The observation that mutant Arg112His exhibits substantial Mdr transport activity provided us with the opportunity to further evaluate the importance of a positive charge at position 112. The pK_a of histidine in proteins in various hydrophilic environments is between 5.6 and 7.0 (*38*). Since, according to the 3D model of MdfA, residue 112 resides on the periplasmic edge of the membrane (TMIV), it might be possible to change the protonation state of a histidine in mutant Arg112His by changing the external pH. Unfortunately, although most appropriate, our direct Ni-NTA based TPP^+ binding assay (see Experimental Procedures) requires basic pH conditions, under which all the R112X mutants lost TPP^+ binding activity (data not shown). Alternatively, we tested the pH effect in vivo. Recent studies have shown that the MdfA-catalyzed transport of neutral substrates (e.g. chloramphenicol) is electrogenic (driven by both ΔpH and $\Delta\psi$), whereas transport of cationic substrates (e.g. EtBr) is electroneutral (driven solely by ΔpH) (*11*). Therefore, decreasing ΔpH (at external basic pH values) has little or no effect on the transport of chloramphenicol by wild-type MdfA. Using a similar approach, we investigated the effects of external pH on the MdfA(Arg112His)-mediated chloramphenicol resistance. The pH-dependent Mdr activity of the wild type and all Arg112 mutants of MdfA is shown in Figure 8. In the absence of chloramphenicol, cells harboring plasmid pT7-5/*mdfA/6His*, each of the mutants, or plain vector grew similarly under all pH conditions. When chloramphenicol was added to the medium, cells expressing the wild-type MdfA were not affected by external pH changes, whereas cells expressing mutants with neutral or negatively charged residues at position 112 (Arg112Cys, Arg112Met, Arg112Gln, and Arg112Glu) were unable to grow under all pH conditions. Remarkably, however, the effect of pH was clearly observed regarding chloramphenicol resistance of cells expressing mutants with positively charged residues at position 112 (Arg112Lys or Arg112His). Although mutant Arg112Lys maintained some chloramphenicol resistance capability only at very acidic pHs, the effect of pH on the function of mutant Arg112His was much stronger. For example, at pH 5.8, the Arg112His mutant grew almost as well as wild-type MdfA. As the pH increased, the growth was less efficient, and at alkaline pH, this mutant completely lost its ability to confer chloramphenicol resistance. These results strongly support the notion that a positive charge at position 112 is essential.

DISCUSSION

MdfA serves as a model for MFS-related secondary Mdr transporters. Several challenging questions regarding its multispecific substrate recognition properties and the bioenergetics of its Mdr transport activity have been resolved to some extent using genetic and biochemical tools. However, better understanding the mechanism underlying Mdr transport by MdfA requires 3D structural information. Here we described the construction of a 3D model for MdfA, its implications, and the consequent identification and characterization of an essential membrane-embedded positive charge.

High-resolution structures of two MFS transporters became recently available: the lactose permease (LacY) (*18*) and the glycerol-3-phosphate transporter (GlpT) (*19*) from *Escherichia coli*. The sequence identity between GlpT and LacY is only ~18%, and their mechanism of action appears to be different, since the former utilizes the downhill gradient of phosphate for an obligatory exchange with Glycerol-Pi (antiporter) while the latter cotransports β-galactosides with

protons (simporter). Despite these differences and the low sequence similarity, both structures show a highly similar fold, which is, in general, similar to the overall structure of another MFS transporter OxlT, based on EM images (*20*). Cα-RMSD between the structurally conserved regions of the two proteins is only 3.7 Å. These findings suggest the intriguing possibility that the fold of these transporters constitutes a scaffold for all MFS transporters with 12 helices. While the fold is conserved, the specific function is obtained by varying sets of amino acids at the substrate binding and translocation domains. In this regard, since MdfA and other MFS Mdr transporters differ substantially from solute-specific transporters, the possibility that they all have a similar fold in the membrane is even more surprising.

Homology modeling is not a good predictive tool at low levels of sequence similarity. Therefore we introduced here an additional tool (kPROT) (*29*) to predict the angular orientation of the 12 TMs in the membrane. According to the results, kPROT performs well for the two MFS transporters of known 3D structure, namely, LacY and GlpT, thus further justifying the usefulness of this approach. Notably, the performance of kPROT is better with GlpT than with LacY, possibly because more intramembrane kinks and twists are present in LacY, and the kPROT analysis disregards such structural irregularities and therefore seems to perform better for perpendicular unbroken helices. Nevertheless, the results confirmed the conjecture that analogous TMs in the two proteins and in MdfA have similar membrane exposure properties. This was concluded from the calculated average kPROT values for each TM in all three proteins. Based on these results, we proposed that the helix packing in MdfA might be similar to that of LacY or GlpT, and we used the kPROT-predicted angular orientation of the TMs, as an important constraint while the 3D model was refined. A similar strategy can be very useful for homology modeling of other membrane proteins, provided that the X-ray structures of representative homologues have been resolved.

The 3D model suggests interesting structural and also functional features in MdfA, several of which have previously been predicted by genetic and biochemical studies. First, a large cavity is observed in the 3D model. This cavity is exposed to the cytoplasmic side of the protein; this is probably the putative multidrug recognition pocket of MdfA (*15*). The cavity formed is very similar in size and shape to that of GlpT (*19*) and somewhat smaller than that of LacY (*18*). This is surprising, because previous results demonstrated that MdfA can bind two substrate molecules simultaneously (*39*). Therefore, we propose that the multidrug recognition pocket of MdfA is very flexible, and this proposal must be evaluated further by X-ray crystallography of the substrate-bound transporter. Interestingly, the cavity in the 3D model of MdfA is negatively decorated by three acidic residues: Glu26, D34, and Asp132, all of them known to play a role in multidrug recognition (*9*, *13*, *17*). The presence of a negatively charged pathway might be required for electrostatic interactions with cationic substrates, which probably represent the majority of MdfA substrates. Notably a similar involvement of acidic residues was identified in the X-ray structures of soluble multidrug binding proteins (*40*, *41*). However, MdfA also has other noncharged substrates, which tolerate dramatic charge substitutions in the pocket (*13*). Therefore, we propose that the negatively charged cavity does not reflect structural constraints. Also in support of the proposal that the observed cavity represents the multidrug recognition pocket of MdfA is the fact that many other recognition-related residues point into this region. Among these residues that were identified as second site suppressors of inactive Glu26 mutants, Gly39, Thr56, and Val54 form a cluster in the periplasmic narrow edge of the cavity. This cluster was implicated in substrate release (*15*). Others, for example, residues Val23, Tyr127, Ala128, Met146, Ala147, Ala150, Val231, and Leu268, are scattered throughout the cavity, mainly on TMs I, IV, V, and some of them were implicated in substrate attraction and binding (*15*). Interestingly, cross-linking studies, which suggested that the cytolasmic loop connecting TMX and TMXI is located at the cytoplasmic opening of the cavity (*16*), are in a good agreement with the 3D model of MdfA. Specifically, the model supports the biochemically measured distance between Glu26 and Val335. Furthermore, the correlated mutation results are also highly consistent with these findings, since the same loop (TMX−TMXI) and its flanking TMs show many correlated mutations with the cavity-forming N-terminal domains of MdfA.

As noted earlier, the 3D model also suggests new structural and functional features that have not been predicted by genetic and biochemical studies. Significantly, the model predicts that many of the TMs are longer than previously thought (*3*, *14*). This new feature has dramatic functional implications, mainly regarding the location of charged residues inside TMs. In addition to the previously predicted membrane-embedded residue Glu26, by lengthening the TMs, specifically TMI and TMIV, two more charged residues are now located within the membrane. In addition, the position of Glu26 has been moved from the periplasmic side of TMI toward its cytoplasmic side. These changes thus created the previously discussed negatively charged, putative multidrug recognition pocket of MdfA. Moreover, the introduction of the remarkably conserved positively charged residue into TMIV and the fact that a similarly positioned arginine is important for function of the tetracycline transporter TetA (*42*) prompted a detailed analysis of the importance of Arg112 in Mdr transport by MdfA. Theoretically, two possible implications can be considered, both related to the proposed proximal position of Asp34 and Arg112. First, a structurally important charged pair could be formed between these residues. Second, Arg112 could function in proton recognition by MdfA similarly to Arg302 in LacY (*43*). The first possibility has been ruled out by neutralizing Asp34 (*17*), and by additional mutagenesis studies where Asp34 and Arg112 were replaced by each other (mutant Asp34Arg/Arg112Asp). The double mutant is not functional (data not shown). The second possibility, which was also approached experimentally, revealed that a positive charge at position 112 is essential for Mdr transport by MdfA although its involvement in the mechanism differs from that of R302 of LacY.

Initially, several mutations at position 112 revealed that only conservative replacements do not completely abolish multidrug resistance and transport activity. Among the conserved mutations, the Arg112His mutant was substantially more active than Arg112Lys. Since the protonation (and thus the charge) of a histidine residue can sometimes be affected by the external pH, the function of MdfA Arg112His was

analyzed by drug resistance assays under various pH conditions. As described, although this mutant functions efficiently in an acidic or neutral environment, basic pH conditions abolish its chloramphenicol resistance activity. Therefore, we concluded that a positive charge is indeed required at position 112. However, the proposal that Arg112 is a functional analogue of Arg302 in LacY could not be confirmed by substrate binding assays. Unlike neutral Arg302 mutants of LacY, which maintain substrate binding activity (*43*), neutralized MdfA Arg112 mutants are completely defective in TPP^+ binding, albeit under alkaline pH conditions (data not shown). These experiments should be repeated once we have a pH-independent binding assay. In any case, because of the above-described results and the high conservation of this residue in the drug−proton antiporter family, it is possible that Arg112 participates in the mechanism of proton recognition by MdfA. Since there are no other charged residues in the putative C-terminal membrane lobe of MdfA, it is possible that the substrate and the proton binding sites overlap to some degree as shown for the small multidrug transporter EmrE (*44*). In the future, this issue will be examined quantitatively, using new tools for substrate binding experiments that could be useful in a wide range of pH conditions.

In summary, the results of the kPROT analysis and the successful construction of a 3D model for MdfA strongly support the prediction that MFS transporters generally have a similar fold in the membrane (*21*−*25*). The 3D model of MdfA, as presented here, further substantiates important previous predictions regarding the mechanism underlying Mdr transport. (i) MdfA has a complex multidrug recognition pocket with exceptional capabilities for interacting with neutral and positively charged compounds. (ii) In addition to TMs I, II, IV, and V, which form the cytoplasmically accessible cavity (the proposed multidrug recognition pocket of MdfA), the loop connecting TMs X and XI has also been identified as a putative substrate recognition determinant. However, in addition to supporting previous conclusions, the 3D model introduced several new research directions regarding the multidrug recognition capacity and the mechanism of proton recognition and translocation by MdfA. The main new features identified in the model are (i) longer TMs compared with previous predictions, and (ii) the two newly identified membrane-embedded charged residues (Asp34 and Arg112). Better understanding of the role of the charged residues inside TMs of MdfA is expected to shed light on the Mdr transport mechanism, as well as on the function of MdfA in alkaline pH homeostasis through its proposed Na^+-$(K^+)/H^+$ antiport activity (*12*, *45*).

ACKNOWLEDGMENT

We are grateful to Ilana Lavie, Orly Noivirt, and Amnon Horovitz for their help in the kPROT and correlated mutation analyses, respectively. We thank Oded Lewinson for critically reading the manuscript.

SUPPORTING INFORMATION AVAILABLE

Prediction of angular orientation of TMs in LacY and GlpT, as calculated by kPROT. This material is available free of charge via the Internet at http://pubs.acs.org.

REFERENCES

1. Putman, M., van Veen, H. W., and Konings, W. N. (2000) Molecular properties of bacterial multidrug transporters, *Microbiol. Mol. Biol. Rev. 64*, 672−693.
2. Zgurskaya, H. I., and Nikaido, H. (2000) Multidrug resistance mechanisms: Drug efflux across two membranes, *Mol. Microbiol. 37*, 219−225.
3. Edgar, R., and Bibi, E. (1997) MdfA, an *Escherichia coli* multidrug resistance protein with an extraordinary broad spectrum of drug recognition, *J. Bacteriol. 179*, 2274−2280.
4. Saier, M. H., Jr., and Paulsen, I. T. (2001) Phylogeny of multidrug transporters, *Semin. Cell Dev. Biol. 12*, 205−213.
5. Jin, Q., Yuan, Z., Xu, J., Wang, Y., Shen, Y., Lu, W., Wang, J., Liu, H., Yang, J., Yang, F., Zhang, X., Zhang, J., Yang, G., Wu, H., Qu, D., Dong, J., Sun, L., Xue, Y., Zhao, A., Gao, Y., Zhu, J., Kan, B., Ding, K., Chen, S., Cheng, H., Yao, Z., He, B., Chen, R., Ma, D., Qiang, B., Wen, Y., Hou, Y., and Yu, J. (2002) Genome sequence of *Shigella flexneri 2a*: insights into pathogenecity through comparison with genomes of *Escherichia coli* K12 and O157, *Nucleic Acids Res. 30*, 4432−4441.
6. Parkhill, J., Dougan, G., James, K. D., Thomson, N. R., Pickard, D., Wain, J., Churcher, C., Mungall, K. L., Bentley, S. D., Holden, M. T., Sebaihia, M., Baker, S., Basham, D., Brooks, K., Chillingworth, T., Connerton, P., Cronin, A., Davis, P., Davies, R. M., Dowd, L., White, N., Farrar, J., Feltwell, T., Hamlin, N., Haque, A., Hien, T. T., Holroyd, S., Jagels, K., Krogh, A., Larsen, T. S., Leather, S., Moule, S., O'Gaora, P., Parry, C., Quail, M., Rutherford, K., Simmonds, M., Skelton, J., Stevens, K., Whitehead, S., and Barrell, B. G. (2001) Complete genome sequence of a multiple drug resistant *Salmonella enterica* serovar Typhi CT18, *Nature 413*, 848−852.
7. Parkhill, J., Wren, B. W., Thomson, N. R., Titball, R. W., Holden, M. T., Prentice, M. B., Sebaihia, M., James, K. D., Churcher, C., Mungall, K. L., Baker, S., Basham, D., Bentley, S. D., Brooks, K., Cerdeno-Tarraga, A. M., Chillingworth, T., Cronin, A., Davies, R. M., Davis, P., Dougan, G., Feltwell, T., Hamlin, N., Holroyd, S., Jagels, K., Karlyshev, A. V., Leather, S., Moule, S., Oyston, P. C., Quail. M., Rutherford, K., Simmonds, M., Skelton, J., Stevens, K., Whitehead, S., and Barrell, B. G. (2001) Genome sequence of *Yersinia pestis*, the causative agent of plague, *Nature 413*, 523−527.
8. Bohn, C., and Bouloc, P.(1998) The *Escherichia coli* cmlA gene encodes the multidrug efflux pump Cmr/MdfA and is responsible for isopropyl-beta-D-thiogalactopyranoside exclusion and spectinomycin sensitivity, *J. Bacteriol. 180*, 6072−6075.
9. Adler, J., Lewinson, O., and Bibi, E. (2004) Role of a conserved membrane-embedded acidic residue in the multidrug transporter MdfA, *Biochemistry 43*, 518−525.
10. Mine, T., Morita, Y., Kataoka, A., Mizushima, T., and Tsuchiya, T. (1998) Evidence for chloramphenicol/H^+ antiport in Cmr (MdfA) system of *Escherichia coli* and properties of the antiporter, *J. Biochem. (Tokyo) 124*, 187−193.
11. Lewinson, O., Adler, J., Poelarends, G. J., Mazurkiewicz, P., Driessen, A. J., and Bibi, E. (2003) The *Escherichia coli* multidrug transporter MdfA catalyzes both electrogenic and electroneutral transport reactions, *Proc. Natl. Acad. Sci. U.S.A. 100*, 1667−1672.
12. Lewinson, O., Padan, E., and Bibi, E. (2004) Alkalitolerance: a biological function for a multidrug transporter in pH homeostasis, *Proc. Natl. Acad. Sci. U.S.A. 101*, 14073−14078.
13. Edgar, R., and Bibi, E. (1999) A single membrane-embedded negative charge is critical for recognizing positively charged drugs by the *Escherichia coli* multidrug resistance protein MdfA, *EMBO J. 18*, 822−832.
14. Adler, J., and Bibi, E. (2002) Membrane topology of the multidrug transporter MdfA: complementary gene fusion studies reveal a nonessential C-terminal domain, *J. Bacteriol. 184*, 3313−3320.
15. Adler, J., and Bibi, E. (2004) Determinants of substrate recognition by the *Escherichia coli* multidrug transporter MdfA identified on both sides of the membrane, *J. Biol. Chem. 279*, 8957−8965.
16. Adler, J., and Bibi, E. (2005) Promiscuity in the geometry of electrostatic interactions between the *Escherichia coli* multidrug resistance transporter MdfA and cationic substrates, *J. Biol. Chem. 280*, 2721−2729.
17. Sigal, N., Molshanski-Mor, S., and Bibi, E. (2005) Proton recognition by the secondary multidrug transporter MdfA, submitted for publication.

18. Abramson, J., Smirnova, I., Kasho, V., Verner, G., Kaback, H. R., and Iwata, S. (2003) Structure and mechanism of the lactose permease of *Escherichia coli*, *Science 301*, 610−615.
19. Huang, Y., Lemieux, M. J., Song, J., Auer, M., and Wang, D. N. (2003) Structure and mechanism of the glycerol-3-phosphate transporter from *Escherichia coli*, *Science 301*, 616−620.
20. Hirai, T., Heymann, J. A., Shi, D., Sarker, R., Maloney, P. C., and Subramaniam, S. (2002) Three-dimensional structure of a bacterial oxalate transporter, *Nat. Struct. Biol. 9*, 597−600.
21. Vardy, E., Arkin, I. T., Gottschalk, K. E., Kaback, H. R., and Schuldiner, S. (2004) Structural conservation in the Major Facilitator Superfamily as revealed by comarative modeling, *Protein Sci. 13*, 1832−1840.
22. Almqvist, J., Huang, Y., Hovmoller, S., and Wang, D. N. (2004) Homology modeling of the human microsomal glucose 6-phosphate transporter explains the mutations that cause the glycogen storage disease type Ib, *Biochemistry 43*, 9289−9297.
23. Salas-Burgos, A., Iserovich, P., Zuniga, F., Vera, J. C., and Fischbarg, J. (2004) Predicting the three-dimensional structure of the human facilitative glucose transporter glut1 by a novel evolutionary homology strategy: insights on the molecular mechanism of substrate migration, and binding sites for glucose and inhibitory molecules, *Biophys. J. 87*, 2990−2999.
24. Wood, J. M., Culham, D. E., Hillar, A., Vernikovska, Y. I., Liu, F., Boggs, J. M., and Keates, R. A. (2005) A Structural Model for the Osmosensor, Transporter, and Osmoregulator ProP of *Escherichia coli*, *Biochemistry 44*, 5634−5646.
25. Lagerstedt, J. O., Voss, J. C., Wieslander, A., and Persson, B. L. (2004) Structural modeling of dual-affinity purified Pho84 phosphate transporter, *FEBS Lett. 578*, 262−268.
26. Hirai, T., Heymann, J. A., Maloney, P. C., and Subramaniam, S. (2003) Structural model for 12-helix transporters belonging to the major facilitator superfamily, *J. Bacteriol. 185*, 1712−1718.
27. Thompson, J. D., Higgins, D. G., and Gibson, T. J. (1994) CLUSTAL W: improving the sensitivity of progressive multiple sequence alignment through sequence weighting, positions-specific gap penalties and weight matrix choice, *Nucleic Acids Res. 22*, 4673−4680.
28. Rost, B. (1996) PHD: predicting one-dimensional protein structure by profile based neural networks, *Methods Enzymol. 266*, 525−539.
29. Pilpel, Y., Ben-Tal, N., and Lancet, D. (1999) kPROT: a knowledge-based scale for the propensity of residue orientation in transmembrane segments. Application to membrane protein structure prediction, *J. Mol. Biol. 294*, 921−935.
30. Henikoff, S., and Henikoff, J. G. (1992) Amino acid substitution matrices from protein blocks, *Proc. Natl. Acad. Sci. U.S.A. 89*, 10915−10919.
31. Notredame, C., Higgins, D. G., and Heringa, J. (2000) T-COFFEE: A novel method for fast and accurate multiple sequence alignment, *J. Mol. Biol. 302*, 205−217.
32. Hirai, T., and Subramaniam, S. (2004) Structure and transport mechanism of the bacterial oxalate transporter OxlT. *Biophys. J. 87*, 3600−3607.
33. Sali, A., and Blundell, T. L. (1993) Comparative protein modelling by satisfaction of spatial restraints, *J. Mol. Biol. 234*, 779−815.
34. Gobel, U., Sander, C., Schneider, R., and Valencia, A. (1994) Correlated mutations and residue contacts in proteins, *Proteins 18*, 309−317.
35. Yerushalmi, H., and Schuldiner, S. (2000) An essential Glutamyl residue in EmrE, a multidrug antiporter from *Escherichia coli*, *J. Biol. Chem. 275*, 5264−5269.
36. Bibi, E., Gros, P., and Kaback, H. R. (1993) Functional expression of mouse mdr1 in *Escherichia coli*, *Proc. Natl. Acad. Sci. U.S.A. 90*, 9209−9213.
37. Hunte, C., Screpanti, E., Venturi, M., Rimon, A., Padan, E., and Michel, H. (2005) Structure of a Na+/H+ antiporter and insights into mechanism of action and regulation by pH, *Nature 435*, 1197−1202.
38. White, A., Handler, P., and Smith, E. L. (1973) In *Principles of biochemistry*, 5th ed., p 120, McGraw-Hill, New York.
39. Lewinson, O., and Bibi, E. (2001) Evidence for simultaneous binding of dissimilar substrates by the *Escherichia coli* multidrug transporter MdfA, *Biochemistry 40*, 12612−12618.
40. Zheleznova, E. E., Markham, P. N., Neyfakh, A. A., and Brennan, R. G. (1999) Structural basis of multidrug recognition by BmrR, a transcription activator of a multidrug transpoter, *Cell 96*, 353−362.
41. Schumacher, M. A., Miller, M. C., Grkovic, S., Brown, M. H., Skurray, R. A., and Brennan, R. G. (2001) Structural mechanisms of QacR induction and multidrug recognition, *Science 294*, 2158−2163.
42. Kimura, T., Nakatani, M., Kawabe, T., and Yamaguchi, A. (1998) Roles of conserved arginine residues in the metal-tetracycline/H+ antiporter of *Escherichia coli*, *Biochemistry 37*, 5475−5480.
43. Abramson, J., Iwata, S., and Kaback, H. R. (2004) Lactose permease as a paradigm for membrane transport proteins, *Mol. Membr. Biol. 21*, 227−236.
44. Yerushalmi, H., and Schuldiner, S. (2000) A model for coupling of H(+) and substrate fluxes based on "time-sharing" of a common binding site, *Biochemistry 39*, 14711−14719.
45. Krulwich, T. A., Lewinson, O., Padan, E., and Bibi, E. (2005) Do physiological roles foster persistence of drug/multidrug-efflux transporters? A case study, *Nat. Rev. Microbiol. 3*, 566−572.

BI051574P